

TSception: Capturing Temporal Dynamics and Spatial Asymmetry from EEG for Emotion Recognition

Yi Ding, *Student Member, IEEE*, Neethu Robinson, *Member, IEEE*, Qiuhaio Zeng, and Cuntai Guan, *Fellow, IEEE*

Abstract—In this paper, we propose TSception, a multi-scale convolutional neural network, to learn temporal dynamics and spatial asymmetry from affective electroencephalogram (EEG). TSception consists of dynamic temporal, asymmetric spatial, and high-level fusion Layers, which learn discriminative representations in the time and channel dimensions simultaneously. The dynamic temporal layer consists of multi-scale 1D convolutional kernels whose lengths are related to the sampling rate of the EEG signal, which learns its dynamic temporal and frequency representations. The asymmetric spatial layer takes advantage of the asymmetric neural activations underlying emotional responses, learning the discriminative global and hemisphere representations. The learned spatial representations will be fused by a high-level fusion layer. With robust nested cross-validation settings, the proposed method is evaluated on two publicly available datasets DEAP and AMIGOS. And the performance is compared with prior reported methods such as FBFgMDM, FBTSC, Unsupervised learning, DeepConvNet, ShallowConvNet, and EEGNet. The results indicate that the proposed method significantly ($p < 0.05$) outperforms others in terms of classification accuracy. The proposed methods can be utilized in emotion regulation therapy for emotion recognition in the future. The source code can be found at: <https://github.com/deepBrains/TSception-New>

Index Terms—Deep Learning, convolutional neural networks, electroencephalography, emotion recognition.



1 INTRODUCTION

EMOTIONS are fundamental factors in human beings' daily life [1], affecting decision-making, perception, human interaction, and human intelligence [2]. Emotion recognition plays an important role in Cognitive Behavioural Therapy (CBT) [3], Emotion Regulation Therapy (ERT)/Emotion-Focused Therapy (EFT) [4] [5] [6], and the evaluation of medicine treatment [7] for emotion-related mental disorders, such as Generalized anxiety disorder (GAD) [8], and Depression [9]. With the potential applications in CBT and EFT, enabling artificial intelligence (AI) to identify human emotions has captured more and more interest from researchers recently [1].

Electroencephalography (EEG) is one of the widely used brain imaging technologies, which measures human brain activity directly. Several electrodes are placed on the surface of the human head to collect EEG signals. EEG contains more comprehensive information regarding human mental state and objective evaluation compared to other emotional signals, such as facial expressions and natural languages. A brain-computer interface (BCI) system can perceive human emotions through EEG, with the help of machine learning and signal processing technologies [10]. Recently, using EEG-BCI has gained popularity among researchers [1] [11]. Atkinson *et al.* [12] improved the SVM classifier accuracy for emotion detection by selecting features efficiently, with

the accuracy being 73.14%. Zheng *et al.* [13] used a discriminative graph regularized extreme learning machine to investigate stable patterns over time from DE features of emotional EEG. Li *et al.* [14] utilized phase-locking value to construct emotion-related brain networks with multiple feature fusion to detect emotions from EEG. Recently, deep learning-based methods have shown promising results in BCI domain, such as motor imagery classification [15] [16] [17] [18] [19], emotion recognition [20] [21] [22] [23], and mental-task classification [24] [25] [26]. Yang *et al.* [20] proposed a hierarchical network structure to perform emotion classification, proposing sub-network nodes to enhance the performance. Li *et al.* [21] constructed EEG into 2D images and proposed a Hierarchical Convolutional Neural Networks (HCNN) to extract the spatial pattern of the EEG. Li *et al.* [22] applied 18 kinds of linear and non-linear features to solve the cross-subject emotion recognition problems, achieving 59.06% and 83.33% on two public datasets.

Although many machine learning methods have been proposed for emotion recognition, most of them highly rely on hand-crafted features. Schirmer *et al.* [15] proposed deep and shallow convolutional neural networks, named DeepConvNet and ShallowConvNet, to process raw EEG data. Both of them have the capabilities of feature extraction and classification with the utilization of CNNs. Lawhern *et al.* [18] proposed EEGNet, an end-to-end deep learning framework that uses three convolutional layers to extract the temporal and spatial patterns from raw EEG data. EEG signal contains abundant brain activity information in different frequency bands [27]. All of the three networks apply single-scale 1D convolutional kernels along the time

- Yi Ding, Neethu Robinson, Qiuhaio Zeng, and Cuntai Guan are with the School of Computer Science and Engineering, Nanyang Technological University, 50 Nanyang Avenue, Singapore, 639798. E-mail: (ding.yi, nrobinson, qiuhaio.zeng, ctguan)@ntu.edu.sg.

Cuntai Guan is the Corresponding Author.

dimension to extract temporal information. To extract the spatial information in EEG signals, previous methods [15] [18] use a 1D convolutional kernel whose length is the same as the number of EEG channels to extract the global spatial pattern. Due to the non-stationary and dynamic nature of EEG, a fixed single kernel may not effectively capture the neural processing underlying emotions that may occur at different time scales and duration. Similarly, a global spatial kernel may not extract the distinct asymmetric EEG patterns which is a known characteristic of emotional processing of brain [28]. Hence, to address these shortcomings, a dynamic temporal layer with different scaled convolutional kernels is proposed to learn richer time-frequency representations with the inspiration of the Inception block of GoogleNet [29]. Besides the global kernel, we take the brain emotional asymmetry into kernel design, a hemisphere kernel whose length equals to the number of EEG channels located on the right/left hemisphere is proposed to extract the hemisphere asymmetric pattern. The effectiveness of multi-scale convolutional neural network is preliminarily explored in our previous work [30]. We further propose a high-level fusion layer after asymmetric spatial layer to further learn from combined hemisphere-global representations to distinct emotion-class specific information.

In this paper, we proposed TSception, a network to capture temporal dynamics and spatial asymmetry from emotional EEG. Parallel multi-scale temporal/spatial kernels in each temporal/spatial layer are designed to enrich the learned temporal/frequency representations and capture emotion asymmetry patterns. A high-level fusion layer is designed to further learn from the hemisphere/global representations of EEG. To evaluate the proposed TSception, we conduct emotion classification experiments on two publicly available benchmark datasets, a Database for Emotion Analysis using Physiological signals (DEAP) [31], and A Dataset for Affect, Personality and Mood Research on Individuals and Groups (AMIGOS) [32]. A robust nested cross-validation is utilized to avoid testing data leakage and biased evaluation. TSception is compared with several deep and non-deep state-of-the-art methods in BCI domain, namely FBFgMDM [33], FBTSC [33], Unsupervised learning [34], DeepConvNet [15], ShallowConvNet [15], EEGNet [18]. From the experiment results, TSception achieves the highest accuracy in EEG emotion recognition experiments. After statistical analysis, extensive ablation studies are conducted to analyze the contribution of each part in TSception. Saliency map [35] is utilized to get the most informative part of the EEG data identified by the network. The results show the network mainly learns from frontal areas, which is commonly known as a functional brain area related to the emotional cognitive process [1]. The averaged saliency map of all subjects shows a right hemisphere lateralization pattern, which is consistent with neuroscience [36] [37].

The major contribution of this work can be summarised as:

- We design TSception, a multi-scale convolutional neural network, which uses multi-scale temporal/spatial convolution kernels to capture temporal dynamics and spatial asymmetry.
- The proposed method is compared with several state

of the art methods in BCI domain, namely FBFgMDM [33], FBTSC [33], Unsupervised learning [34], DeepConvNet [15], ShallowConvNet [15], EEGNet [18]. Extensive ablation studies are conducted to better understand the proposed TSception.

The PyTorch implementation of TSception is available at <https://github.com/deepBrains/TSception-New>

The remainder of this article is organized as follows. Some related works will be introduced in Section II. In Section III the details of TSception are introduced. Section IV describes the datasets and experiment settings. The result and analysis will be given in Section V, Finally, we discuss and come to conclusions in Section VI.

2 RELATED WORK

2.1 GoogleNet and Inception Block

Inception block is first introduced in GoogleNet [29], the winner of the 2014-ILSVRC competition. Instead of using single-size convolutional kernels in each convolutional layer, multi-scale kernels are utilized with the split, transform and merge operations in the inception block. With the help of the inception block, GoogleNet improved the learning of varying represents for the same object in different images.

2.2 Convolutional Neural Networks for EEG Data

Recently the convolutional neural networks (CNNs) have shown promising results in BCI [38] [39] [18]. Instead of using EEG as 2D time series, Li *et al.* [21] used the relative location of the electrodes to rearrange the channel dimension of EEG to map each channel on a sparse 2D location map. The channels in the paper refer to the EEG electrodes instead of RGB dimensions in images or the input/output channels for convolutional layers, if not specified. The 2D map can reflect the spatial pattern of the EEG, hence (n, n) sized convolutional kernels can be applied to it as the typical convolution on images, where $n \in [1, 3, 5, 7, \dots]$ is the length/width of the convolutional kernel. The local spatial pattern is captured through sharing of kernels. However, one drawback is that the global spatial information is not well extracted since n is usually small which gives a small perception range. Schirrmester *et al.* [15] proposed deep and shallow convolutional neural networks, named DeepConvNet and ShallowConvNet, to process raw EEG data, combining the feature extraction and classification using a 2 stage spatial and temporal input convolution layer. Robinson *et al.* [38] presented a deep CNN architecture that extracts dynamic spatial interaction between spectral regions of EEG to decode hand motor imagery. Fahimi *et al.* [24] proposed an inter-subject transfer learning framework using CNNs to detect attentive mental state. Recently, Lawhern *et al.* [18] proposed EEGNet, which extracts spatial information by the depth-wise convolution kernel whose size is $(n, 1)$. Letting n being the number of channels, the global spatial dependency can be learned. In EEGNet, there are also single-scale 1D temporal kernels in a convolutional layer to extract temporal information.

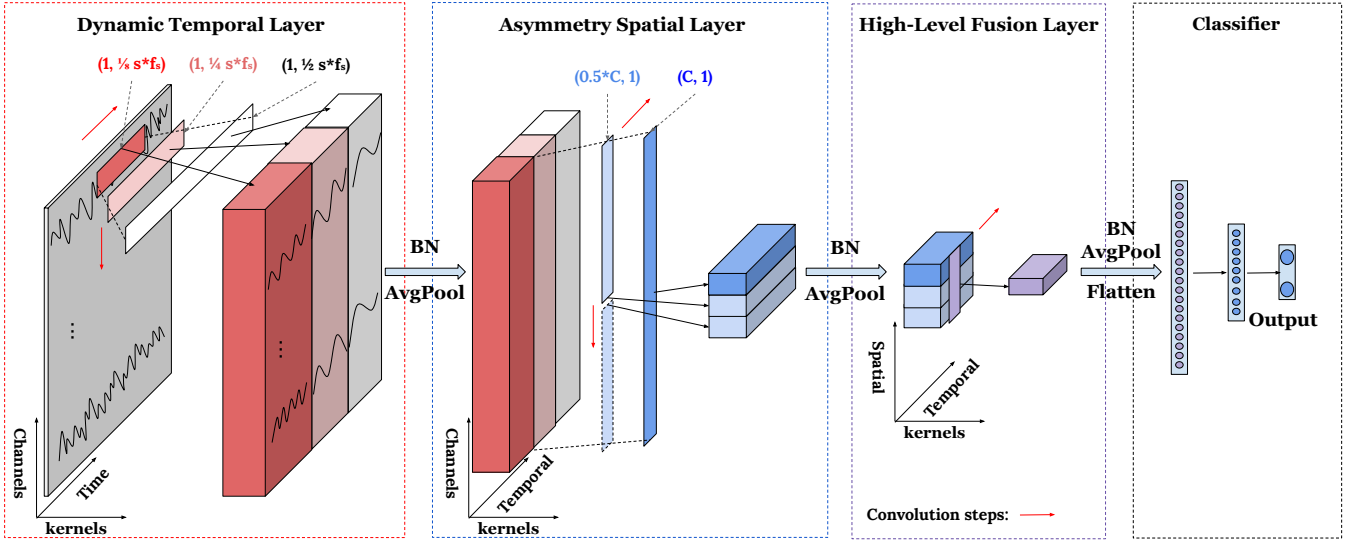


Fig. 1. Structure of TSception. In the figure, f_s is the sampling rate of the EEG signals, C is the number of channels, and BN stands for batch normalization. TSception has four main parts: the dynamic temporal layer, the asymmetric spatial layer, the high-level fusion layer, and the classifier. The dynamic temporal layer will first learn the dynamic temporal/frequency representations from the raw EEG data channel by channel. After getting the learned representations for each channel, the asymmetric spatial layer will be applied to learn the global spatial representations and the emotional asymmetry pattern using different scale convolutional kernels. To fuse the information from hemisphere and global representations, a high-level fusion layer is utilized. Finally, the fused representation will be passed to the fully connected layers with the softmax as the activation function.

3 MULTI-SCALE CONVOLUTIONAL NEURAL NETWORKS

EEG data can be treated as 2D time series, whose dimensions are channels (EEG electrodes) and time respectively. The time dimension reflects the brain activity changes from time to time. The spatial dimension can show the brain activation patterns across different functional areas due to the different locations of the brain. EEG signals contain abundant information in different frequency bands [27]. In order to extract more discriminative time-frequency representations, multi-scale 1D convolutional kernels are utilized in dynamic temporal layer to enrich the learned time-frequency representations. As for asymmetric spatial layer, it takes the advantages of neuroscience finding [28] which indicates the brain activities in right and left hemispheres are not symmetrically related to emotions. A hemisphere kernel is proposed to learn the asymmetric representations among two hemispheres. To learn from the learned representations of both the hemisphere and global kernels, a high-level fusion layer is further proposed. A detailed description of the temporal, spatial, and high-level fusion layers will be discussed in this section.

3.1 Dynamic Temporal Layer

The dynamic temporal layer consists of multi-scale 1D temporal kernels (T kernels). In order to learn dynamic temporal representations, we set the length of the temporal kernels as the specific ratios of sampling rate f_s of EEG. These ratios are defined as $\alpha^i \in \mathbb{R}$, where i is the level of the dynamic temporal layer. i will vary from 1 to L , if the dynamic temporal layer has L levels. Hence s_T^i , the size of T kernels in i -th level, can be defined as:

$$s_T^i = (1, \alpha^i \cdot f_s), i \in [1, 2, 3] \quad (1)$$

From the frequency perspective, in EEGNet, the length of the T kernel is set as half the sampling rate, allowing for capturing frequency information at 2 Hz and above [18]. Activations related to emotions are observed in Alpha (8-12 Hz), Beta (12-30 Hz), and Gamma (>30 Hz) bands [1]. In this work, we expand the temporal perception ranges, letting $L = 3, i = 1$ to 3 and $\alpha = 0.5$, the ratio coefficients will become [0.5, 0.25, 0.125], capturing frequency at 4 Hz to above and 8 Hz to above as well. We hold the hypothesis that the multi-scale temporal kernels can enrich the learned dynamic frequency representations from the raw EEG, providing more emotion-related information. From the time perspective, multi-scale T kernels can capture long short-term temporal patterns, and learn more diverse representations. The higher level T kernel has a smaller ratio coefficient, which gives a shorter convolutional kernel length and vice versa. The long temporal kernel can learn long-term temporal and low-frequency diverse representations. The short kernel extracts short-term temporal and high-frequency representations. Let X denote the raw EEG input sample array. $X = [X^0, X^1, \dots, X^n]$, $X^n \in \mathbb{R}^{c \times l}$, where n is the number of EEG samples, c is the number of channels, l is the length of each sample. By parallelly applying the multi-scale temporal kernels on the input EEG samples, dynamic temporal representations can be generated. After $LeakyReLU(\cdot)$ activation function, the feature map is further down-sampled by average pooling. The reason for using average pooling is to reduce the effect of the noise as well as the feature dimension since EEG signals are of high dimensions with a low signal-noise ratio. Let $Z_{temporal}^i$ denote the output of the i -th level temporal kernel, $Z_{temporal}^i \in \mathbb{R}^{n \times t \times c \times f_i}$, where n is the number of samples, t is the number of each level's T kernel, c is the number of channels, and f_i is the length of the feature after i -th level

convolution operation. $\mathbf{Z}_{temporal}^i$ is defined as:

$$\mathbf{Z}_{temporal}^i = AvgPool(\Phi_{L-ReLU}(Conv1D(\mathbf{X}, s_T^i))) \quad (2)$$

where s_T^i is the T kernel size, \mathbf{X} is the input raw EEG samples array, $Conv1D(\cdot)$ is the 1D convolution operation with the kernel size being s_T^i , step being (1,1), and $\Phi_{L-ReLU}(\cdot)$ is the LeakyReLU(\cdot) activation function.

The output of each level's T kernel will be concatenated along the feature dimension. In order to reduce the internal covariate shift problems in neural networks, batch normalization [40] is added. Hence the final output of the dynamic temporal layer, $\mathbf{Z}_T, \mathbf{Z}_T \in \mathbb{R}^{n \times t \times c \times \sum f_i}$ is defined as:

$$\mathbf{Z}_T = f_{bn}([\mathbf{Z}_{temporal}^1, \dots, \mathbf{Z}_{temporal}^i]), i \in [1, 2, 3] \quad (3)$$

where the f_{bn} is the batch normalization operation, and $[\cdot]$ stands for concatenation operation along the feature (f) dimension.

3.2 Asymmetric Spatial Layer

The asymmetric spatial layer has multi-scale 1D convolutional kernels whose sizes are related to the location of the EEG channels. There are two types of spatial kernels: global kernel, hemisphere kernel.

The global kernel has a size of $(c, 1)$, where c is the number of channels. Since the length of the kernel is the same as the channel dimension of the input EEG segment, it can learn the global spatial information.

In this work, we further combine the frontal area of brain emotional asymmetry [41] into the kernel design. The hemisphere kernel is used to extract the relationship patterns between the left and right hemispheres by sharing the convolutional kernels. The size of the hemisphere kernel is $(0.5 \cdot c, 1)$, and the step is $(0.5 \cdot c, 1)$, where c is the total number of channels. The hemisphere kernel is shared by two hemispheres without overlapping so that the asymmetric pattern can be extracted. The size of the spatial kernel s_S^j can be defined as:

$$s_S^j = (\delta^j \cdot c, 1), j \in [0, 1] \quad (4)$$

where $\delta = 0.5$ is the coefficient to control the ratio between the spatial kernel length and the number of total channels.

Let $\mathbf{Z}_{spatial}^j$ denote the output of the j -th type spatial kernel, $\mathbf{Z}_{spatial}^j \in \mathbb{R}^{n \times s \times c_j \times f}$, where n is the number of samples, s is the number of each type S kernel, c_j is the number of channels after j -th spatial convolution, and f is the length of the feature after each spatial convolution operation. $\mathbf{Z}_{spatial}^j$ is defined as:

$$\mathbf{Z}_{spatial}^j = AvgPool(\Phi_{L-ReLU}(Conv1D(\mathbf{Z}_T, s_S^j))) \quad (5)$$

where s_S^j is the S kernel size, \mathbf{Z}_T is the output of dynamic temporal layer, $Conv1D(\cdot)$ is the 1D convolution operation with the kernel size being s_S^j , step being (1,1), and $\Phi_{L-ReLU}(\cdot)$ is the LeakyReLU(\cdot) activation function.

In order to apply hemisphere kernels, the sequence of channels in the input EEG samples should be carefully arranged. The order of the channels should be $[channel_{left}, channel_{right}]$, where the $channel_{left}$ are the channels located in the left hemisphere, the $channel_{right}$ are the ones on the right hemisphere. The order for channels

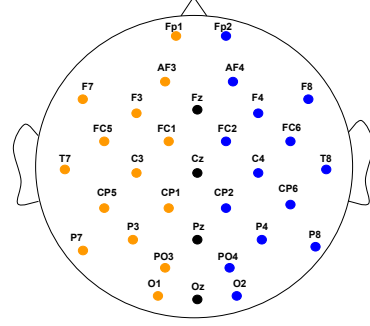


Fig. 2. The location map of 32 channels cap. The electrodes can be divided into 3 groups: electrodes on the left hemisphere(in orange), electrodes on the right hemisphere(in blue), and the electrodes on the central line(in black). For the electrodes located on the central line of the head, Fz, Cz, Pz, and Oz, which can not be paired on left and right hemisphere, we further removed them to let TSception learn the asymmetric pattern of left and right hemispheres better.

on each hemisphere should also be rearranged to make each kernel weight shared between pairs of symmetrically located electrodes on two hemispheres. Because the step of the hemisphere kernel is also $(0.5 \cdot c, 1)$. Fig. 2 shows the electrode locations of DEAP dataset. The final output of the asymmetric spatial layer, $\mathbf{Z}_S, \mathbf{Z}_S \in \mathbb{R}^{n \times s \times \sum c_j \times f}$ is defined as:

$$\mathbf{Z}_S = f_{bn}([\mathbf{Z}_{spatial}^0, \dots, \mathbf{Z}_{spatial}^j]), j \in [0, 1] \quad (6)$$

where f_{bn} is the batch normalization operation, and $[\cdot]$ stands for concatenation operation along the channel (c) dimension. The output of hemisphere kernel have a length of two in the spatial dimension, which refers to two hemispheres respectively. The output of global kernel is only a vector whose length in the spatial dimension is one. After concatenation, the channel dimension is $\sum c_j = 3$.

3.3 High-level Fusion Layer

After the asymmetric spatial layer, two types of representations are learned, the global and hemisphere representations. Global representations reflect the relations among each EEG electrode, while the hemisphere representations show the relations between the left and right hemispheres. In order to learn high-level spatial representations by fusing the learned information from global and hemispheres, the high-level fusion layer is further proposed. Given the output of asymmetric spatial layer, $\mathbf{Z}_S \in \mathbb{R}^{n \times s \times 3 \times f}$, a 1D convolutional layer whose kernel size is $(3, 1)$ is utilized to fuse the information along the spatial dimension. After LeakyReLU(\cdot), average pooling, and batch normalization, the final learned global-hemisphere fusion representations will be generated by:

$$\mathbf{Z}_{fusion} = f_{bn}(AvgPool(\Phi_{L-ReLU}(Conv1D(\mathbf{Z}_S, (3, 1)))) \quad (7)$$

Finally, the latent representation of \mathbf{Z}_{fusion} will be fed into fully connected layers after dropout function, $\Phi_{dp}(\cdot)$, and ReLU(\cdot) activation function. The final output layer is activated by the softmax function, $\Phi_{softmax}(\cdot)$. Hence the final output can be calculated by:

$$\mathbf{Output} = \Phi_{softmax}(W' \Phi_{dp}(\Phi_{ReLU}(W(\Gamma(\mathbf{Z}_S)) + b)) + b') \quad (8)$$

where the $\Gamma(\cdot)$ is the flatten operation, W and W' are the trainable weight matrix, b and b' are the bias terms.

Finally the proposed TSception can be summarised in **Algorithm 1**.

Algorithm 1: TSception

Input: Raw EEG data $X^n \in \mathbb{R}^{c \times l}$; ground truth label y ;
Output: $pred$, the prediction of TSception

- 1 Initialization;
- 2 **do in sequential**
- 3 # get the output of the dynamic temporal layer
- 4 **for** $i \leftarrow 1$ **to** 3 **do**
- 5 get i -th temporal kernel size by Eq. 1;
- 6 get $z_{temporal}^i$ by Eq. 2 using X^n as input;
- 7 **end**
- 8 get Z_T by Eq. 3;
- 9 # get the output of the asymmetric spatial layer
- 10 **for** $j \leftarrow 0$ **to** 1 **do**
- 11 get j -th temporal kernel size by Eq. 4;
- 12 get $z_{spatial}^j$ by Eq. 2 using Z_T as input;
- 13 **end**
- 14 get Z_S by Eq. 6;
- 15 # get the output of the high-level fusion layer
- 16 get Z_{fusion} by Eq. 7;
- 17 **end**
- 18 get $pred$ using Eq. 8;

Return: $pred$

4 EXPERIMENTS

4.1 Datasets

To evaluate the proposed TSception, we conducted several experiments on two publicly available benchmark datasets, a Database for Emotion Analysis using Physiological signals (DEAP)¹ [31], and A Dataset for Affect, Personality and Mood Research on Individuals and Groups (AMIGOS)² [32]. TABLE 1 summarizes the related information of the two datasets used in our experiments.

DEAP is a multi-modal human affective states dataset, including EEG, facial expressions, and galvanic skin response (GSR). There are 32 subjects watching music video clips while their EEG, facial expression, and GSR are recorded. Each of the subjects participates in 40 trials in total. The duration of each trial is 1 minute with a 3 seconds pre-trial baseline. After each trial, the subject will be given a questionnaire to provide their own emotional state in arousal, valence, dominance, and liking with each dimension having 9 discrete levels. The EEG is collected using 32 channels device, with the sampling rate being 512Hz.

AMIGOS was proposed to study affect, personality traits, and mood using EEG signals. Different from DEAP, AMIGOS has two types of experiment protocols: one is for individuals and another one conducts experiments within groups of subjects. Both short and long emotional videos are utilized as stimuli to study the effect of the stimulus

duration on emotion responses. There are 40 subjects who participated in the experiments. Each of them watched 16 short emotional videos in the individual experiments. In the group studies, 4 long videos were selected as the stimuli with some of the subjects alone and the rest in groups. Electroencephalogram (EEG), Electrocardiogram (ECG), and Galvanic Skin Response (GSR) were recorded using wearable sensors. The emotions have been annotated with self-assessment of affective levels felt by the participants and external assessment.

TABLE 1

Summary of related information of the datasets used in the experiments

Factor	DEAP	AMIGOS
Subjects	32	40
Stimuli	Music videos	Emotional videos
Trials/subject	40	16
Trial duration	1 min	-
EEG channels	32	14
Sampling rate	512Hz	128Hz
Label	V/A/L	V/A

V: valence; A: arousal; L:liking

-: the trial duration varies from 51s to 150s on AMIGOS

4.2 Pre-processing

For DEAP, the 3 seconds pre-trial baseline was removed for each trial. Then the data was down-sampled from 512Hz to 128Hz, after which the electrooculogram (EOG) was removed as [31]. To remove the low-high frequency noise, a band-pass filter from 4.0-45Hz was applied to the original EEG. Finally, the EEG channels were averaged to the common reference. The class label for each dimension is from 1 to 9, hence 5 was selected as a threshold to project the 9 discrete value into low and high classes in each dimension as [31] [33]. In this study, only arousal and valence dimensions are considered to be comparable with [33]. Liking dimension is added in the experiment to compare our results with [34], and dominance dimension is not included in the experiments since it only has single class. The processed data was fed into the deep learning methods directly instead of using the manually extracted features.

For AMIGOS, only the short video experiments data are utilized for the performance comparison. The data were averaged to the common reference first, after which a 4-45Hz band-pass filter is applied to remove the low and high frequency noise. Arousal and valence dimensions are selected to evaluate the performance of different methods. 5 is selected as the threshold to get high/low arousal and valence. The trial contains the abnormal value is discarded. Since the trials in AMIGOS vary in duration, the last 1 min's data of each trial is selected as the input sample as DEAP.

4.3 Experiment Settings

To avoid testing data leakage problems and solve chance level shifting issue caused by the unbalanced classes, we follow [33], a "leave one trial out" cross-validation is adopted for each subject. In each cross-validation step, one trial is selected as testing data and the rest are selected as training

1. <http://www.eecs.qmul.ac.uk/mmv/datasets/deap/index.html>

2. <http://www.eecs.qmul.ac.uk/mmv/datasets/amigos/index.html>

data. The process is repeated till every trial is selected as testing data once for each subject. The average accuracy of all subjects is reported as the final evaluation criterion as [33] [31]. To avoid biased evaluation, nested cross-validation [42] is utilized. The inner loop of nested cross-validation is 5-fold cross-validation to get a more generalized evaluation. Hence after selecting one trial as testing data, the remaining data will be divided into five folds for 5-fold cross-validation. The detailed training strategy will be introduced in the subsection Training Strategy.

As suggested by [33], the unbalanced classes issue for DEAP dataset should also be considered. Since ‘5’ is selected as the threshold to get low/high arousal and valence, the classes will become unbalanced, which causes the chance level shifting issue for accuracy. To make the classes balanced, an up-sampling strategy is utilized as [33]. The trials in the class which has a smaller number of trials will be randomly duplicated to make the number of trials equal in both low and high arousal/valence classes. After up-sampling, there will be 40-68 trials/class for each subject. After balancing the classes, the leave one trial out cross-validation is conducted.

4.4 Training Strategy

A two-stage training strategy is adopted to take full use of the training data. In the first stage, one trial of the subject is selected as testing data, then a 5-fold cross-validation will be applied to the remaining training data. The remaining training data is divided into five folds using a balance sampler which can ensure that the classes in each fold are balanced. In each time, one fold is selected as validation data, the remaining four folds are training data. The model which achieves the best accuracy on validation data among the five folds will be saved as a candidate model. In the second training stage, the best model on the validation set is selected as the initial model of the second training stage. The model will be fine-tuned for five epochs on the entire training data to generate the final model for testing. The average accuracy of 5 fold will be the validation accuracy for hyper-parameter selecting. Since the model is already trained in the first stage, the learning rate in the second stage will be scaled by 0.1. As such, the testing data never participate in these two training stages in any form as suggested by [34].

4.5 Implementation Details

The code is implemented using PyTorch library, the source code can be found via this link³.

The number of temporal and spatial kernels in dynamic temporal, asymmetric spatial, and high-level fusion layer is equal to 10. The number of hidden nodes in the first fully connected layer is chosen as 32. For model training, the maximum training epoch of the first stage is 25 while the one for stage II is 5 instead. SGD optimizer is utilized to optimize the training process with the initial learning rate being 1e-2 and momentum being 0.9. A learning rate scheduler is also added whose step is 5. Cross-entropy loss is selected as the loss function to guide the training process.

3. <https://github.com/deepBrains/TSception-New>

Algorithm 2: Two-stage Training Strategy

Input: Raw EEG data $X = [X^0, \dots, X^i]$ for each subject, where $i \in \mathbb{R}$ is the trial index, the total trials of the subject $trial_{total}$, ground truth label Y , balance-sampler $\psi(\cdot)$, model $\phi(\cdot)$, loss function $L_{\epsilon}(\cdot)$, learning rate lr , the maximum training epochs $epoch_{max}$, accuracy calculation function $f(\cdot)$

- 1 Initialization;
- 2 **while** $i < trial_{total}$ **do**
- 3 **Stage I:**
- 4 $X_{test}, Y_{test} = X^i, Y^i$;
- 5 $X_{train}, Y_{train}, X_{val}, Y_{val} = \psi_{0.8}(X_{rest}, Y_{rest})$;
- 6 $acc_{max} = 0$; $epoch = 0$;
- 7 **while** $epoch < epoch_{max}$ **do**
- 8 $loss = L_{\epsilon}(\phi(X_{train}), Y_{train})$;
- 9 $back_propagation(loss, lr)$;
- 10 $acc_{val} = f(\phi(X_{val}), Y_{val})$;
- 11 **if** $acc_{val} > acc_{max}$ **then**
- 12 $acc_{max} = acc_{val}$;
- 13 save model as $\phi_{max-acc}$;
- 14 **else**
- 15 $epoch+ = 1$;
- 16 **Stage II:**
- 17 $X_{comb}, Y_{comb} =$
- 18 $cat((X_{train}, X_{val})), cat((Y_{train}, Y_{val}))$;
- 19 $epoch = 0$;
- 20 **while** $epoch < epoch_{max-comb}$ **do**
- 21 $loss = L_{\epsilon}(\phi(X_{comb}), Y_{comb})$;
- 22 $back_propagation(loss, lr * 0.01)$;
- 23 $acc = f(\phi(X_{comb}), Y_{comb})$;
- 24 **if** $epoch == epoch_{max-comb}$ **then**
- 25 save model as ϕ_{final} ;
- 26 **else**
- 27 $epoch+ = 1$;
- 27 $acc_{test} = f(\phi(X_{test}), Y_{test})$

For more details, please refer to the open-access GitHub repository for TSception.

5 RESULTS AND ANALYSIS

In this section, the results of the ‘‘Leave one trial out’’ cross-validation on DEAP and AMIGOS datasets will be presented. We first present the accuracies of the proposed and the compared methods with a statistical comparison of the results. Then ablation studies are presented to understand the contribution of each component in TSception. Finally, saliency maps are presented to show that the most informative part of the EEG identified by the network is the frontal areas of the brain for all 32 subjects in DEAP dataset. The averaged saliency map of 32 subjects shows strong activation in the frontal area and right hemisphere lateralization.

5.1 Statistical Analysis

Table 2 shows the classification results for different methods on DEAP dataset using ‘‘leave one trial out’’ cross-

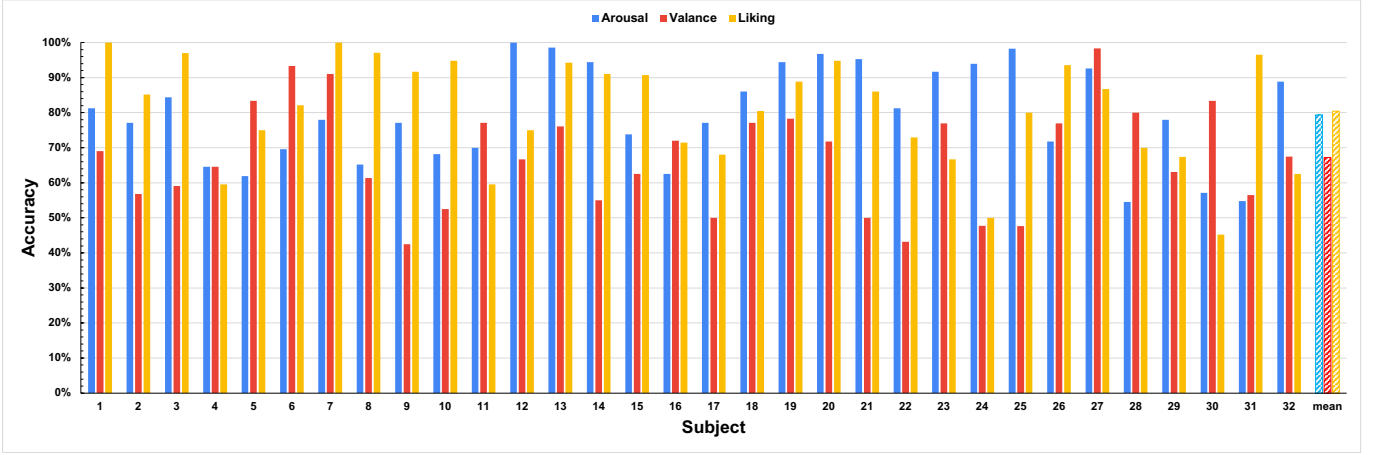


Fig. 3. Mean accuracy of each subject for arousal, valence, and liking using TSception.

TABLE 2
Comparison against classification accuracy on leave one trial out experiments on DEAP

Method	<i>Arousal</i>	std	<i>Valence</i>	std	<i>Liking</i>	std
FBFgMDM [33]	60.04% ***	–	61.01% *	–	–	–
FBTSC [33]	60.60% ***	–	61.09% *	–	–	–
Unsupervised Learning [34]	61.17% ***	–	54.61% ***	–	65.08% ***	–
DeepConvNet [15]	72.21% ***	13.56%	62.80% *	11.79%	74.33% ***	12.88%
ShallowConvNet [15]	72.39% ***	11.41%	63.02% *	11.88%	74.01% ***	12.97%
EEGNet [18]	74.03% ***	14.98%	66.25%	13.67%	76.71% *	13.72%
TSception(ours)	79.34%	13.92%	67.22%	14.82%	80.44%	15.07%

p -value between the method and TSception: * indicating ($p < 0.05$), ** indicating ($p < 0.01$), *** indicating ($p < 0.001$).

TABLE 3
Classification results of TSception, EEGNet, ShallowConvNet, and DeepConvNet on AMIGOS

Method	<i>Arousal</i>	std	<i>Valence</i>	std
DeepConvNet	68.67% **	17.84%	61.13%	16.97%
ShallowConvNet	69.36% *	18.16%	60.43%	16.70%
EEGNet	72.43%	18.47%	59.61%	14.52%
TSception(ours)	75.03%	15.31%	61.38%	14.13%

p -value between the method and TSception: * indicating ($p < 0.05$), ** indicating ($p < 0.01$), *** indicating ($p < 0.001$).

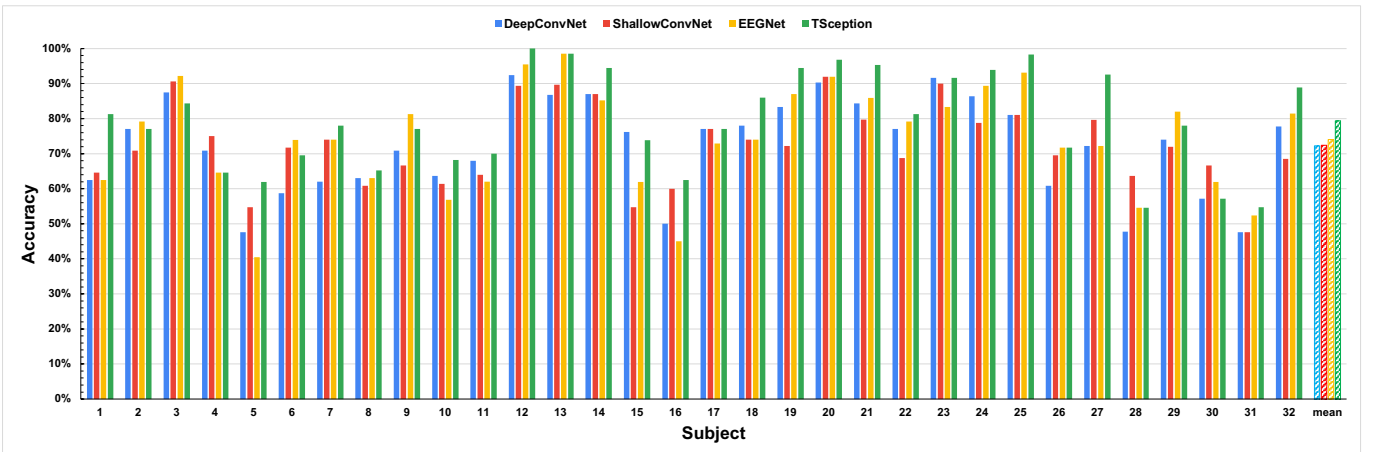


Fig. 4. Mean accuracy of each subject for arousal on DEAP.

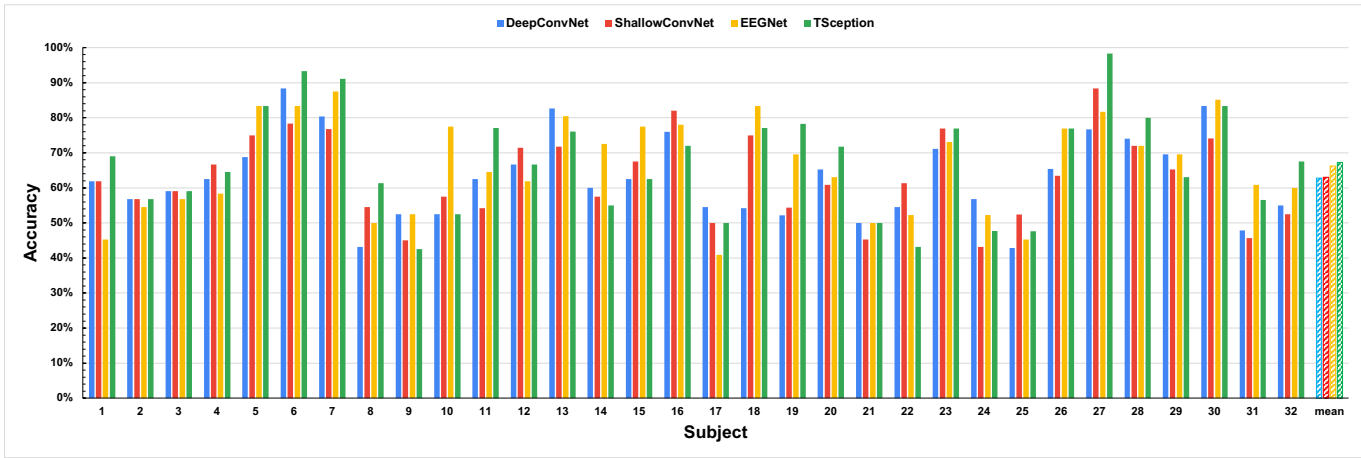


Fig. 5. Mean accuracy of each subject for valence on DEAP.

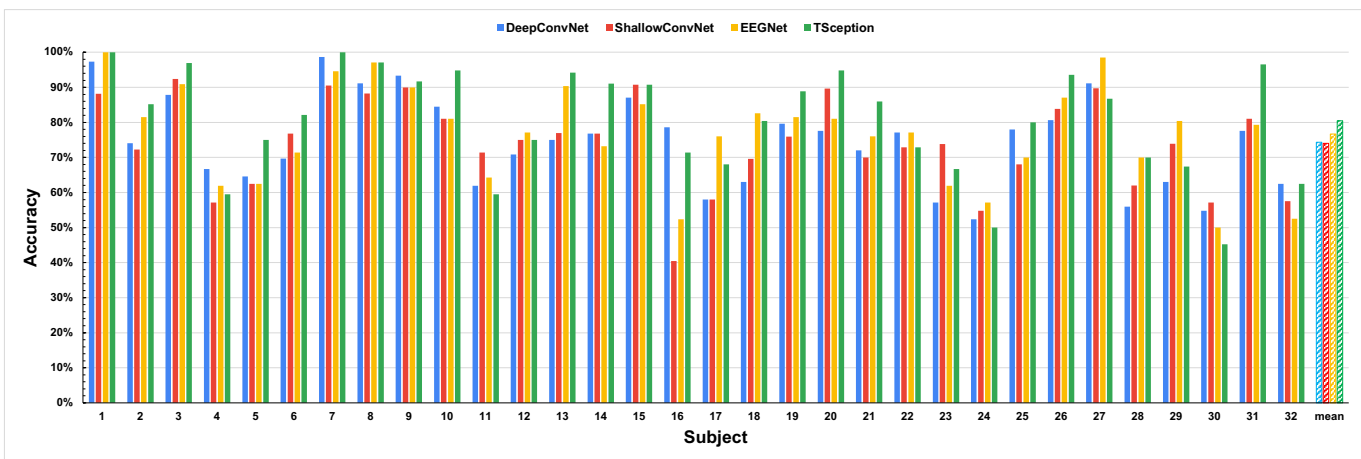


Fig. 6. Mean accuracy of each subject for liking on DEAP.

validation. To conduct statistical analysis, a two-tailed Wilcoxon Signed-Rank Test is utilized. Compared with non-deep learning methods, FBFgMDM, FBTSC, and Unsupervised Learning, all the deep learning methods achieve higher classification accuracies, showing the effectiveness of deep learning methods. Among deep learning methods, which learn representations from raw EEG signals, TSception achieves the best performance for all three dimensions, with the accuracy being 79.34% for arousal, 67.22% for valence, and 80.44% for liking respectively. EEGNet achieves second place compared with the other methods (74.03% for arousal, 66.25% for valence, and 76.71% for liking). The accuracy of TSception for arousal is 5.31% higher than EEGNet ($p < 0.001$), the one for valence has 0.97% improvement over EEGNet ($p = 0.4777$), and the one for liking achieves 3.73% higher accuracy than EEGNet ($p < 0.05$). Compared with ShallowConvNet, which is the third place method, TSception achieves 6.95% improvement for arousal ($p < 0.001$), 4.2% improvement for valence ($p = 0.0173 < 0.05$), and 6.43% improvement for liking ($p < 0.001$). TSception also gets 7.13%, 4.42%, and 6.11% higher than DeepConvNet for arousal, valence, and liking, with the p -value being < 0.00001 , 0.0214, and 0.0007 respectively. Fig. 3 shows the mean accuracy of leave-one-

trial-out cross-validation for each subject using TSception. The classification accuracies of the three dimensions vary for each subject. The best accuracy for arousal and liking are all equal to 100% (subject 12 for arousal, subject 1, and subject 7 for liking), while the best accuracy for valence is 98.33% for subject 27. All the deep learning methods achieve better accuracies for the liking dimension, while the accuracies for valence are all relatively low ($< 70\%$), indicating valence is harder to correctly classified than arousal and liking. Fig. 4 - Fig. 6 show the performance of different deep learning methods on each subject for arousal, valence, and liking respectively. The order of subjects is the same as the DEAP official order.

According to Table 3, TSception still achieves the highest accuracies for both arousal and valence but with much lower values (75.03% for arousal, and 61.38% for valence). EEGNet has the second place for arousal (72.42%) but the last place for valence (59.61%). Deep and Shallow ConvNet have almost similar performance for arousal and valence, with the accuracies being 68.67% for arousal 61.13% for valence, and 69.36% for arousal 60.43% for valence. All the deep learning have close performances for valence dimension, but this time the lowest accuracy is achieved by EEGNet (59.61%). Fig. 7 and Fig. 8 show the classification

accuracies for each subject using different deep learning methods. Some subjects have a single class if we choose 5 as the threshold as [33] [34], in this study, those single class subjects are removed for evaluation. From Fig. 7 and Fig. 8, the classification accuracies of EEGNet, ShallowConvNet, and DeepConvNet have relatively larger variance among different subjects. The best accuracies of TSception, EEGNet, and DeepConvNet for arousal are all equal to 100%.

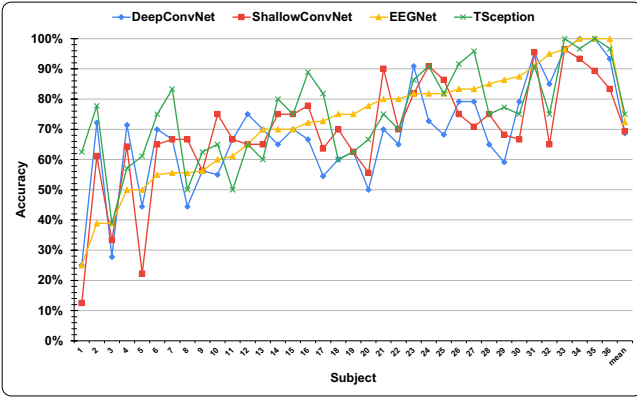


Fig. 7. Mean accuracy of each subject for arousal on AMIGOS. The results are sorted using the accuracies of EEGNet for better visualization.

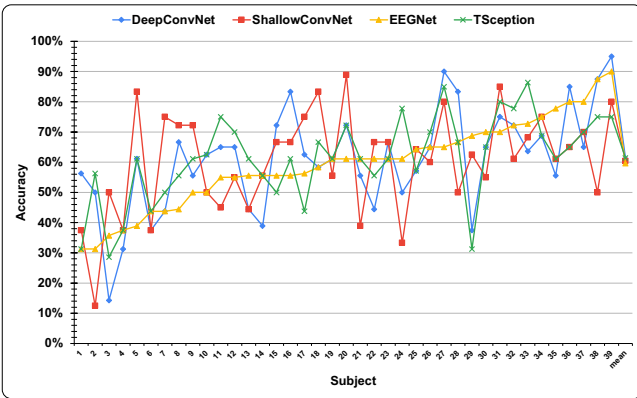


Fig. 8. Mean accuracy of each subject for valence on AMIGOS. The results are sorted using the accuracies of EEGNet for better visualization.

5.2 Ablation Study

The proposed method TSception has dynamic temporal layer, asymmetric spatial layer, and high-level fusion layer three functional parts. dynamic temporal layer learns the dynamic temporal/frequency representations for each channel; asymmetric spatial layer extracts the spatial pattern cross channels, especially the emotional asymmetry pattern; the high-level fusion layer fuses the learned global and hemisphere representations as well as reduces the dimension of the hidden feature maps. The combination of those three parts leads to the success of classification tasks. Ablation studies are conducted to further understand which part contributes more to the improvement of classification accuracies. Each time, one of the dynamic temporal layer, asymmetric spatial layer, and high-level fusion layer is removed to see the changes in classification accuracies.

DEAP dataset is used for the ablation study since the overall performance is higher than AMIGOS.

The results of the ablation study are shown in Table 4. Almost all of the accuracies drop after removing any of the three types of layers, indicating all components contribute to the improvement of classification, except when the asymmetric spatial layer is removed, the accuracy for valence slightly increases by 0.95%, which is not significant compared with the accuracy drops for other dimensions. According to the table, the most significant drops of accuracy for three dimensions are observed when the dynamic temporal layer is removed from TSception with the decrements being 8.38%, 2.03%, and 13.5% for arousal, valence, and liking. This demonstrated that the dynamic temporal layer contributes more than the other two layers, especially for the liking dimension, the drop is the largest in the ablation study. The asymmetric spatial layer contributes more for arousal and liking since the accuracies drop from 79.34% to 76.44% for arousal, and from 80.44% to 76.32% for liking if the asymmetric spatial layer is removed. However, the accuracy slightly increases for valence, indicating the contribution of asymmetric spatial layer for valence is less than the other two dimensions. Although the drops of accuracy for three dimensions after removing the high-level fusion layer are relatively less than removing the other two types of layers, the drops still show the contribution of the high-level fusion layer. The high-level fusion layer contributes more to liking because the accuracy decreases by 3.44% after removing it.

According to the above ablation studies, dynamic temporal layer contributes more to the classification improvements. To study the contribution of multi-scale 1D temporal kernels, the single-scale temporal kernel in dynamic temporal layer is evaluated on DEAP dataset. Each time, one type of temporal kernel is kept to compare with the original TSception that has multi-scale temporal kernels in its dynamic temporal layer. The results are shown in Table 5. The lengths of the 1D convolutional kernel of T1, T2, and T3 are $0.5s \times f_s$, $0.25s \times f_s$, and $0.125s \times f_s$ respectively. The accuracies for arousal and liking are all decreased for signal-scale temporal kernel settings. For arousal, the drops of accuracy are 4.79%, 2.71%, 4.63% for only keeping T1, T2, and T3. For liking, only keeping T1, T2, or T3 all causes the downgrade of the neural networks, with the decreases being 3.88%, 2.51%, and 4.51%. Although the accuracies for valence all increase with single-scale kernels, the increase is still less than the overall impact across all three classifications, indicating the effectiveness of multi-scale temporal kernels.

5.3 Interpretability

In this part, the saliency map [43] is utilized to visualize which parts of the data are more informative. The Saliency map is one of the most commonly used tools to intuitively show which regions of the input have the classification-related information. To better visualize the saliency map, the original saliency map is averaged along the time dimension to get the topological map of the EEG channels. The normalized saliency maps of different trials of each subject are averaged to get the mean saliency map of the subject

TABLE 4
Results of ablation study of TSception on DEAP

DT	AS	HF	<i>Arousal</i>	changes	<i>Valence</i>	changes	<i>Liking</i>	changes
✓	✓	✓	70.96%	-8.38%	65.20%	-2.03%	67.39%	-13.5%
✓	✓	✓	76.44%	-2.90%	68.18%	+0.95%	76.32%	-4.12%
✓	✓	✓	77.37%	-1.97%	66.06%	-1.17%	77.00%	-3.44%
✓	✓	✓	79.34%	-	67.22%	-	80.44%	-

DT: dynamic temporal layer; AS: asymmetric spatial layer; HF: high-level fusion layer
 ✓: keep the component
 changes: compared with the original TSception

TABLE 5
Results of ablation study of multi-scale 1D kernel in dynamic temporal layer on DEAP

T1	T2	T3	<i>Arousal</i>	changes	<i>Valence</i>	changes	<i>Liking</i>	changes
✓			74.56%	-4.79%	69.36%	+2.14%	76.56%	-3.88%
	✓		76.63%	-2.71%	70.55%	+3.33%	77.93%	-2.51%
		✓	74.72%	-4.63%	67.60%	+0.38%	75.94%	-4.51%
✓	✓	✓	79.34%	-	67.22%	-	80.44%	-

T1: length = 0.5s; T2: length = 0.25s; T3: length = 0.125s
 ✓: keep the component
 changes: compared with the original TSception

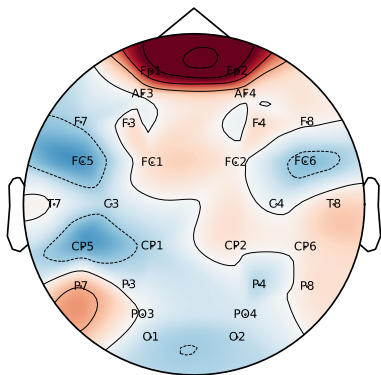


Fig. 9. Averaged saliency map of all 32 subjects in DEAP dataset. The most informative region identified by the neural network is the frontal area, which is in deep red. There is also a right hemisphere lateralization pattern in the averaged saliency map. The name of EEG electrodes are also plotted for better visualization.

for general visualization. The mean saliency maps of all 32 subjects in DEAP dataset are shown in Fig. 10. From the results, the most informative region identified by the neural network is the frontal area for all subjects. This is consistent with previous works [44] [45] [46], which indicates the network learns from the proper region. According to the saliency maps of 32 subjects, most of the subjects show right hemisphere lateralization, especially subject 13, subject 19, subject 20, subject 21, and subject 30, which show strong lateralization patterns in their saliency maps. The saliency maps of all 32 subjects are further averaged to get the overall pattern information. The mean saliency map of all the subjects is shown in Fig. 9, which shows strong activation in the frontal area, and right hemisphere lateralization. Besides the frontal area, the right hemisphere lateralization is consistent with the neuroscience [36] [37] that the right hemisphere has a special role in emotion in

the intact brain. This further indicates the neural network learns emotion-related information from the raw EEG data.

6 DISCUSSION AND CONCLUSION

Accurate detection of emotion has huge potential usage in real-world applications, especially in healthcare, such as Cognitive Behavioural Therapy, Emotion Regulation Therapy/Emotion-Focused Therapy for emotion-related mental disorders. Most of the previous works highly rely on the human extracted features, which requires too much domain knowledge. Deep learning, especially convolutional neural networks, has the auto feature-extracting ability. In this work, a multi-scale convolutional neural network is proposed to learn temporal dynamics and spatial asymmetry patterns from raw EEG data. For EEG data, there are mainly two types of information to learn, temporal and spatial information respectively. Typically 1D convolution will be applied to the temporal and spatial dimension of EEG data separately to learn those two types of information as [15] [18]. EEG is non-station and dynamic in temporal dimension, a single 1D convolutional kernel may not capture such temporal dynamics effectively. To learn the neural processing underlying emotions that may occur at different time scales and duration, multi-scale temporal convolutional kernels are proposed to build the dynamic temporal layer. Different from DeepConvNet, ShallowConvNet, and EEGNet, besides a global spatial kernel which may not effectively extract the distinct asymmetric EEG patterns [28], a hemisphere kernel is also proposed to learn the asymmetric pattern better. After learning the global and hemisphere representations by the asymmetric spatial layer, a high-level fusion layer is designed to fuse the information from two types of representations. According to the results on two public datasets shown in Table 2 and Table 3, the proposed TSception achieves the best classification accuracies for all dimensions with the accuracies being 79.34%, 67.22%, and

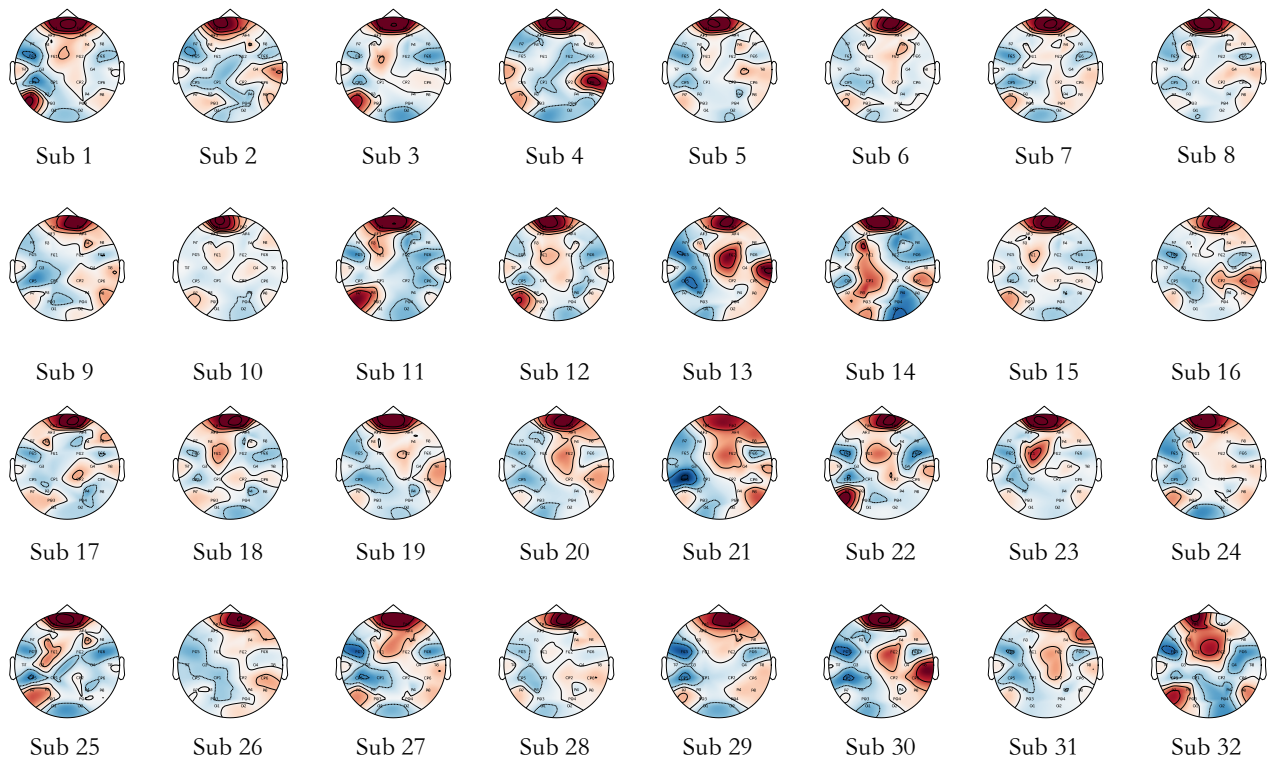


Fig. 10. Saliency maps of all 32 subjects in DEAP dataset. The saliency map is averaged along the time dimension to plot the topological map.

80.44% for arousal, valence, and liking on DEAP dataset, indicating the effectiveness of the proposed method for emotion recognition. All the deep learning methods perform better than the compared machine learning methods, even learning from raw data directly. However, all the deep learning methods perform relatively bad for the valence dimension, with all the accuracies being less than 70% (a common threshold in BCI for evaluation), indicating the valence is harder to classify than arousal which is consistent with [47] [48].

For the experiments, data deviation and evaluation metrics are the most important factors to consider. In the BCI domain, there are chopped and non-chopped experiments for EEG data [15]. The chopped experiment will use a sliding window with or without overlapping to cut each trial’s EEG data into shorter segments. The non-chopped ones use each trial’s data as the input to the classifier directly [33]. As suggested by [34], in chopped experiments, if the samples among different trials are randomly shuffled before dividing the data into training and test data, one can get very high accuracies since the data within each trial is very similar compared with other trials [49]. Hence the experiments in this paper follow [33], which use one trial’s data as one input sample to the classifier, and a leave-one-trial-out cross-validation is utilized. For a more robust evaluation of the networks, nested cross-validation [42] is further adopted with the inner loop being 5-fold cross-validation and the outer loop being leave-one-trial-out cross-validation. With nested cross-validation, the test data can be isolated from training data while training and hyper-parameters fine-tuning, avoiding test data leakage issue. The test data is selected in the outer loop, but the training

and hyper-parameter selection are in the inner loop. Subject-specific experiments are conducted as [34] using the above cross-validation settings. As for evaluating metrics, we also follow the suggestion of [33] to overcome the unbalanced class problems for accuracy to avoid change level shifting issue.

After getting the classification results, each component of TSception is removed separately to study the contribution of them. According to the ablation study results shown in Table 4, the dynamic temporal layer contributes more than the other two layers, indicating there is more information in the temporal dimension. Especially for arousal and liking, the drops of accuracies are 8.38% and 13.5% after removing the dynamic temporal layer. The asymmetric spatial layer contributes more to arousal and liking. Although the contribution of the high-level fusion layer is the smallest, it can reduce the size of the hidden activation map, which further reduces the model size consequently. Since the dynamic temporal layer contribute more than others, an ablation study of the dynamic temporal layer is further conducted to study the contribution of multi-scale temporal kernels. If we only keep either of the three scale temporal kernels, the accuracies will drop, showing the ability of multi-scale temporal convolutional kernels. To make sure the neural network learns the emotion-related information instead of irrelevant features, saliency maps are acquired to visualize the most informative region identified by the neural network itself. The saliency maps of 32 subjects all show strong activation in the frontal area, which is commonly know as a functional area reflecting the emotional responses in the brain [50] [1]. This is consistent with another EEG study [44]. A right hemisphere lateralization pattern is also observed in

the averaged saliency map of all subjects, which is consistent with neuroscience [36] [37] that the right hemisphere has a special role in emotional process in the brain.

Although TSception achieves relatively higher classification accuracies than the baselines, the limitation of this work should also be considered. In this work, only subject-specific experiments are conducted, the generalization ability cross subjects is not well explored. Another limitation is that only non-chopped experiments are conducted. The performance of TSception on chopped experiments is still unknown. It's worth mentioning that randomly shuffle cross-trial issues in chopped experiments should also be carefully arranged to avoid overestimation.

In this paper, TSception, a multi-scale convolutional neural network, is proposed to capture temporal dynamics and spatial asymmetry for EEG emotion recognition. Using a robust nested cross-validation strategy, the proposed method and several baseline methods are evaluated on two publicly available benchmark datasets. The results on two public datasets show the superior of the proposed TSception. In the future, the generalization ability of TSception cross subjects will be explored. The effect of segment length in chopped experiments on TSception should also be considered and studied.

ACKNOWLEDGMENTS

This work was partially supported by the RIE2020 AME Programmatic Fund, Singapore (No. A20G8b0102).

REFERENCES

- [1] S. M. Alarcão and M. J. Fonseca, "Emotions recognition using EEG signals: A survey," *IEEE Transactions on Affective Computing*, vol. 10, no. 3, pp. 374–393, July 2019.
- [2] R. J. Dolan, "Emotion, cognition, and behavior," *Science*, vol. 298, no. 5596, pp. 1191–1194, 2002.
- [3] J. K. Carpenter, L. A. Andrews, S. M. Witcraft, M. B. Powers, J. A. J. Smits, and S. G. Hofmann, "Cognitive behavioral therapy for anxiety and related disorders: A meta-analysis of randomized placebo-controlled trials," *Depression and Anxiety*, vol. 35, no. 6, pp. 502–514, 2018.
- [4] D. M. Fresco, D. S. Mennin, R. G. Heimberg, and M. Ritter, "Emotion regulation therapy for generalized anxiety disorder," *Cognitive and Behavioral Practice*, vol. 20, no. 3, pp. 282 – 300, 2013.
- [5] L. Greenberg, "Emotion-focused therapy," *Clinical Psychology & Psychotherapy*, vol. 11, no. 1, pp. 3–16, 2004.
- [6] R. D. Lane, L. Ryan, L. Nadel, and L. Greenberg, "Memory reconsolidation, emotional arousal, and the process of change in psychotherapy: New insights from brain science," *Behavioral and Brain Sciences*, vol. 38, p. e1, 2015.
- [7] E. S. Herbener, S. K. Hill, R. W. Marvin, and J. A. Sweeney, "Effects of antipsychotic treatment on emotion perception deficits in first-episode schizophrenia," *American Journal of Psychiatry*, vol. 162, no. 9, pp. 1746–1748, 2005.
- [8] H. Goodwin, J. Yiend, and C. R. Hirsch, "Generalized anxiety disorder, worry and attention to threat: A systematic review," *Clinical Psychology Review*, vol. 54, pp. 107 – 122, 2017.
- [9] R. S. Duman, G. K. Aghajanian, G. Sanacora, and J. H. Krystal, "Synaptic plasticity and depression: new insights from stress and rapid-acting antidepressants," *Nature Medicine*, vol. 22, no. 3, pp. 238–249, 2016.
- [10] S. K. Ehrlich, K. R. Agres, C. Guan, and G. Cheng, "A closed-loop, music-based brain-computer interface for emotion mediation," *PLOS ONE*, vol. 14, no. 3, pp. 1–24, 03 2019.
- [11] A. Craik, Y. He, and J. L. Contreras-Vidal, "Deep learning for electroencephalogram (EEG) classification tasks: a review," *Journal of Neural Engineering*, vol. 16, no. 3, p. 031001, apr 2019.
- [12] J. Atkinson and D. Campos, "Improving BCI-based emotion recognition by combining EEG feature selection and kernel classifiers," *Expert Systems with Applications*, vol. 47, pp. 35 – 41, 2016.
- [13] W. Zheng, J. Zhu, and B. Lu, "Identifying stable patterns over time for emotion recognition from EEG," *IEEE Transactions on Affective Computing*, vol. 10, no. 3, pp. 417–429, July 2019.
- [14] P. Li, H. Liu, Y. Si, C. Li, F. Li, X. Zhu, X. Huang, Y. Zeng, D. Yao, Y. Zhang, and P. Xu, "EEG based emotion recognition by combining functional connectivity network and local activations," *IEEE Transactions on Biomedical Engineering*, vol. 66, no. 10, pp. 2869–2881, Oct 2019.
- [15] R. T. Schirrmester, J. T. Springenberg, L. D. J. Fiederer, M. Glasstetter, K. Eggenesperger, M. Tangermann, F. Hutter, W. Burgard, and T. Ball, "Deep learning with convolutional neural networks for EEG decoding and visualization," *Human Brain Mapping*, vol. 38, no. 11, pp. 5391–5420, 2017.
- [16] O. Kwon, M. Lee, C. Guan, and S. Lee, "Subject-independent brain-computer interfaces based on deep convolutional neural networks," *IEEE Transactions on Neural Networks and Learning Systems*, pp. 1–14, 2019.
- [17] Y. R. Tabar and U. Halici, "A novel deep learning approach for classification of EEG motor imagery signals," *Journal of Neural Engineering*, vol. 14, no. 1, p. 016003, nov 2016.
- [18] V. J. Lawhern, A. J. Solon, N. R. Waytowich, S. M. Gordon, C. P. Hung, and B. J. Lance, "EEGNet: a compact convolutional neural network for EEG-based brain-computer interfaces," *Journal of Neural Engineering*, vol. 15, no. 5, p. 056013, Jul 2018.
- [19] S. Sakhavi, C. Guan, and S. Yan, "Learning temporal information for brain-computer interface using convolutional neural networks," *IEEE Transactions on Neural Networks and Learning Systems*, vol. 29, no. 11, pp. 5619–5629, Nov 2018.
- [20] Y. Yang, Q. M. J. Wu, W. Zheng, and B. Lu, "EEG-based emotion recognition using hierarchical network with subnetwork nodes," *IEEE Transactions on Cognitive and Developmental Systems*, vol. 10, no. 2, pp. 408–419, June 2018.
- [21] J. Li, Z. Zhang, and H. He, "Hierarchical convolutional neural networks for EEG-based emotion recognition," *Cognitive Computation*, vol. 10, no. 2, pp. 368–380, Apr 2018.
- [22] X. Li, D. Song, P. Zhang, Y. Zhang, Y. Hou, and B. Hu, "Exploring EEG features in cross-subject emotion recognition," *Frontiers in Neuroscience*, vol. 12, p. 162, 2018.
- [23] Y. Li, W. Zheng, Y. Zong, Z. Cui, T. Zhang, and X. Zhou, "A bi-hemisphere domain adversarial neural network model for EEG emotion recognition," *IEEE Transactions on Affective Computing*, pp. 1–1, 2018.
- [24] F. Fahimi, Z. Zhang, W. B. Goh, T.-S. Lee, K. K. Ang, and C. Guan, "Inter-subject transfer learning with an end-to-end deep convolutional neural network for EEG-based BCI," *Journal of Neural Engineering*, vol. 16, no. 2, p. 026007, Jan 2019.
- [25] Z. Jiao, X. Gao, Y. Wang, J. Li, and H. Xu, "Deep convolutional neural networks for mental load classification based on EEG data," *Pattern Recognition*, vol. 76, pp. 582 – 595, 2018.
- [26] Z. Gao, X. Wang, Y. Yang, C. Mu, Q. Cai, W. Dang, and S. Zuo, "EEG-based spatio-temporal convolutional neural network for driver fatigue evaluation," *IEEE Transactions on Neural Networks and Learning Systems*, vol. 30, no. 9, pp. 2755–2763, 2019.
- [27] Kai Keng Ang, Zheng Yang Chin, Haihong Zhang, and Cuntai Guan, "Filter bank common spatial pattern (FBCSP) in brain-computer interface," in *2008 IEEE International Joint Conference on Neural Networks (IEEE World Congress on Computational Intelligence)*, June 2008, pp. 2390–2397.
- [28] J. J. B. Allen, P. M. Keune, M. Schönenberg, and R. Nusslock, "Frontal EEG alpha asymmetry and emotion: From neural underpinnings and methodological considerations to psychopathology and social cognition," *Psychophysiology*, vol. 55, no. 1, p. e13028, 2018.
- [29] C. Szegedy, W. Liu, Y. Jia, P. Sermanet, S. Reed, D. Anguelov, D. Erhan, V. Vanhoucke, and A. Rabinovich, "Going deeper with convolutions," in *The IEEE Conference on Computer Vision and Pattern Recognition (CVPR)*, June 2015.
- [30] Y. Ding, N. Robinson, Q. Zeng, D. Chen, A. A. Phyto Wai, T. S. Lee, and C. Guan, "TSception: a deep learning framework for emotion detection using EEG," in *2020 International Joint Conference on Neural Networks (IJCNN)*, 2020, pp. 1–7.
- [31] S. Koelstra, C. Muhl, M. Soleymani, J. Lee, A. Yazdani, T. Ebrahimi, T. Pun, A. Nijholt, and I. Patras, "DEAP: A database for emotion

- analysis using physiological signals," *IEEE Transactions on Affective Computing*, vol. 3, no. 1, pp. 18–31, 2012.
- [32] J. A. Miranda Correa, M. K. Abadi, N. Sebe, and I. Patras, "AMIGOS: A dataset for affect, personality and mood research on individuals and groups," *IEEE Transactions on Affective Computing*, pp. 1–1, 2018.
- [33] A. Appriou, A. Cichocki, and F. Lotte, "Modern machine-learning algorithms: For classifying cognitive and affective states from electroencephalography signals," *IEEE Systems, Man, and Cybernetics Magazine*, vol. 6, no. 3, pp. 29–38, 2020.
- [34] Z. Liang, S. Oba, and S. Ishii, "An unsupervised EEG decoding system for human emotion recognition," *Neural Networks*, vol. 116, pp. 257 – 268, 2019.
- [35] Y. Zhai and M. Shah, "Visual attention detection in video sequences using spatiotemporal cues," in *Proceedings of the 14th ACM International Conference on Multimedia*, 2006, p. 815–824.
- [36] G. E. Schwartz, R. J. Davidson, and F. Maer, "Right hemisphere lateralization for emotion in the human brain: Interactions with cognition," *Science*, vol. 190, no. 4211, pp. 286–288, 1975.
- [37] S. M. Sheppard, L. M. Keator, B. L. Breining, A. E. Wright, S. Saxena, D. C. Tippett, and A. E. Hillis, "Right hemisphere ventral stream for emotional prosody identification: Evidence from acute stroke," *Neurology*, vol. 94, no. 10, pp. e1013–e1020, 2020.
- [38] N. Robinson, S. Lee, and C. Guan, "EEG representation in deep convolutional neural networks for classification of motor imagery," in *2019 IEEE International Conference on Systems, Man and Cybernetics (SMC)*, Oct 2019, pp. 1322–1326.
- [39] R. Mane, N. Robinson, A. P. Vinod, S. W. Lee, and C. Guan, "A multi-view CNN with novel variance layer for motor imagery brain computer interface," in *2020 42nd Annual International Conference of the IEEE Engineering in Medicine Biology Society (EMBC)*, 2020, pp. 2950–2953.
- [40] S. Ioffe and C. Szegedy, "Batch normalization: Accelerating deep network training by reducing internal covariate shift," *arXiv 1502.03167*, 2015.
- [41] A. B. Craig, "Forebrain emotional asymmetry: a neuroanatomical basis?" *Trends in Cognitive Sciences*, vol. 9, no. 12, pp. 566 – 571, 2005.
- [42] S. Varma and R. Simon, "Bias in error estimation when using cross-validation for model selection," *BMC Bioinformatics*, vol. 7, no. 1, p. 91, 2006.
- [43] K. Simonyan, A. Vedaldi, and A. Zisserman, "Deep inside convolutional networks: Visualising image classification models and saliency maps," *arXiv preprint arXiv:1312.6034*, 2013.
- [44] Y. Li, W. Zheng, L. Wang, Y. Zong, and Z. Cui, "From regional to global brain: a novel hierarchical spatial-temporal neural network model for EEG emotion recognition," *IEEE Transactions on Affective Computing*, 2019.
- [45] P. Shammi and D. T. Stuss, "Humour appreciation: a role of the right frontal lobe," *Brain*, vol. 122, no. 4, pp. 657–666, 1999.
- [46] P. A. Kragel, M. Kano, L. Van Oudenhove, H. G. Ly, P. Dupont, A. Rubio, C. Delon-Martin, B. L. Bonaz, S. B. Manuck, P. J. Gianaros *et al.*, "Generalizable representations of pain, cognitive control, and negative emotion in medial frontal cortex," *Nature neuroscience*, vol. 21, no. 2, pp. 283–289, 2018.
- [47] Y. Liu and O. Sourina, "EEG-based valence level recognition for real-time applications," in *2012 International Conference on Cyberworlds*. IEEE, 2012, pp. 53–60.
- [48] X. Li, P. Zhang, D. Song, G. Yu, Y. Hou, and B. Hu, "EEG based emotion identification using unsupervised deep feature learning," *SIGIR2015 workshop on neuro-physiological methods in IR research*, 2015.
- [49] X. Zhang, J. Liu, J. Shen, S. Li, K. Hou, B. Hu, J. Gao, and T. Zhang, "Emotion recognition from multimodal physiological signals using a regularized deep fusion of kernel machine," *IEEE transactions on cybernetics*, 2020.
- [50] T. A. Dennis and B. Solomon, "Frontal EEG and emotion regulation: Electrocortical activity in response to emotional film clips is associated with reduced mood induction and attention interference effects," *Biological psychology*, vol. 85, no. 3, pp. 456–464, 2010.